

The assessment of aerosol optical properties over Mohal in the northwestern Indian Himalayas using satellite and ground-based measurements and an influence of aerosol transport on aerosol radiative forcing

Raj Paul Guleria · Jagdish Chandra Kuniyal · Pan Singh Rawat · Nand Lal Sharma · Harinder Kumar Thakur · Pitamber Prasad Dhyani · Mahavir Singh

Received: 10 October 2010 / Accepted: 7 June 2011 / Published online: 29 June 2011
© Springer-Verlag 2011

Abstract The present study deals with the aerosol optical properties which are assessed during the period 2007 to 2009 over Mohal (31.9°N, 77.12°E) in the northwestern Indian Himalaya, using ground-based measurements and multi-satellite data. The daily average value of aerosol optical depth (AOD) at 500 nm, Ångström exponent and turbidity coefficient are 0.24 ± 0.08 , 1.02 ± 0.34 and 0.13 ± 0.05 , respectively. The comparative study of satellite and ground-based measurements reveals that the percentage retrieval for daily AOD at 550 nm over Mohal within the expected accuracy ($\Delta\tau_{p,\lambda} = \pm 0.05 \pm 0.15\tau_{p,\lambda}$) is around 87%, with a significant correlation coefficient of 0.76. The present study suggests that the retrieval of AOD through satellite data is able to characterise the distribution of AOD over Mohal. However, further efforts are needed in order to eliminate systematic errors in the existing Moderate Resolution Imaging Spectroradiometer (MODIS) algorithm. The transport of desert dust and anthropogenic

aerosol during high aerosol loading days caused a significant reduction in surface-reaching solar radiation by 149 and 117%, respectively. This large reduction in surface-reaching solar radiation increased the atmospheric heating rate by 0.93 and 0.72 K day⁻¹, respectively. This study indicates significant climatic implications due to the transport of aerosols in the northwestern Indian Himalaya.

1 Introduction

The measurement of aerosol optical properties and their influence on incoming solar radiations are of most concern in climate studies, owing to the role they play in the Earth-atmosphere system (Bellouin et al. 2005; Intergovernmental Panel on Climate Change [IPCC] 2007; Jayaraman et al. 2010). Aerosols affect the incoming and outgoing solar radiation by scattering and absorption processes (Charlson et al. 1992; Kaufman et al. 1998; Satheesh and Ramanathan 2000; Ramachandran et al. 2006; Ranjan et al. 2007; Badarinath et al. 2008). The aerosol optical depth (AOD) is one of the most important optical properties of aerosols, which is directly related to the magnitude of attenuation of direct solar radiation by scattering and absorption processes (Ranjan et al. 2007). The two more general aerosol properties are the Ångström exponent (α) and the turbidity coefficient (β). The Ångström exponent provides general information on the aerosol size distribution. The turbidity coefficient is a measure of the total aerosol loading in the vertical plane and is equal to the AOD at a 1- μm wavelength (Raju et al. 2003). Extensive analysis on the Ångström exponent and its spectral variations have been made by Kaskaoutis et al. (2007), while Jacovides et al. (2005) have analysed both α and β , even in different spectral bands.

Responsible editor: R. Roebeling.

R. P. Guleria · J. C. Kuniyal (✉) · N. L. Sharma · H. K. Thakur
G.B. Pant Institute of Himalayan Environment and
Development, Himachal Unit, Mohal-Kullu 175 126, India
e-mail: jckuniyal@gmail.com; jckuniyal@rediffmail.com

P. S. Rawat
Department of Physics, DSB Campus, Kumaun University,
Nainital 263 002, India

P. P. Dhyani
G.B. Pant Institute of Himalayan Environment and
Development, Kosi-Katarmal, Almora 263 643, India

M. Singh
Department of Physics, Himachal Pradesh University,
Shimla 171 005, India

Aerosols generated at one place are transported over long distances and produce consequent effects on incoming solar radiation at locations far away from the source (Hoppel et al. 1990; Sharma et al. 2010). In this concern, air trajectories play an important role in transporting aerosols (Moorthy et al. 1999; Satheesh et al. 2001; Kaskaoutis et al. 2010; Sharma et al. 2010). The transport pathways of aerosol over India showed the dependence of the trajectory on the air-mass altitude (Badarinath et al. 2007, 2009; Kuniyal et al. 2009). Over India, dust storms are a major climatic phenomenon originating in the Thar Desert and are recognised as a primary source of atmospheric soil dust (Middleton 1986). The Sahara Desert is one of the major sources of mineral aerosols worldwide (Morales 1986). The investigation carried out by Kuniyal et al. (2009) suggests that the northwestern part of the Indian Himalayas is affected due to the transport of aerosols from the Sahara and Thar Deserts.

In recent years, there has been growing concern that aerosols emitting from natural sources, such as volcanic activity, wind-blown dust, sea spray, convection etc., and anthropogenic sources, such as combustion, industrial activity, agricultural waste burning, mining etc. (Kedia and Ramachandran 2009), are major factors causing disturbances in existing weather and climatic conditions over the Indian sub-continent (Menon et al. 2002; Ramanathan et al. 2005; Lau et al. 2006; Gautam et al. 2009). In India, the systematic studies of aerosols are initiated under the Indian Space Research Organization Geosphere Biosphere Programme (ISRO-GBP) (Moorthy et al. 1999). Preliminary results have been published in a number of studies (Moorthy et al. 1998; Narasimhamurthy et al. 1998; Parameswaran et al. 1999; Beegum et al. 2008; Kaskaoutis et al. 2009; Kuniyal et al. 2009).

The application of satellite data to derive the AOD has advanced dramatically in the last few years (King et al. 1999). One of the main advancements is the systematic derivation of the AOD over land and ocean from the Moderate Resolution Imaging Spectroradiometer (MODIS) (Chu et al. 2002). In order to improve the accuracy of the MODIS data set, detailed validation of the MODIS AOD by using the ground-based Multi-wavelength Radiometer (MWR) and Microtops, especially the sun photometers from the Aerosol Robotic Network (AERONET), have been performed by many authors over the Indian sub-continent (Remer et al. 2005; Tripathi et al. 2005; Prasad et al. 2007; Aloysius et al. 2008; Gogoi et al. 2008; Vinoj et al. 2008; Misra et al. 2010; Pathak et al. 2010; Sharma et al. 2010). The validation exercise revealed that there is still error which is caused by the improper treatment of the reflections and aerosol models used in the MODIS aerosol inversion algorithm (Remer et al. 2005; Tripathi et al. 2005; Misra et al. 2008).

Numerous measurements to investigate the aerosol optical properties and impact assessments have been reported from the Indian region in recent years (Moorthy et al. 1999; Satheesh et al. 2001; Dey et al. 2004; Ramachandran et al. 2006; Babu et al. 2007; Aloysius et al. 2008; Gogoi et al. 2008; Badarinath et al. 2009; Kedia et al. 2010; Sharma et al. 2010). However, these measurements are focused either on urban landmass or oceans adjoining densely populated coastal regions. Investigations of aerosol optical properties and their impact assessments from remote and sparsely inhabited regions of mountain ecosystems are very rare. Mohal in the Kullu valley is a semi-urban experimental site in the northwestern Indian Himalaya under the ISRO-GBP MWR network (Kuniyal et al. 2009). The main objective of this nationwide network is to evolve regional aerosol characterisation, incorporating the heterogeneities in space, time and spectral domains to estimate the Aerosol Radiative Forcing over India (ARFI) and to assess its impacts on the regional and global climate. This region of the Indian Himalayas is topographically very fragile and ecologically very delicate. Due to the variety of the ecosystem, surface conditions and aerosol properties, in-situ observations of aerosols in this part of the Himalayas have become very important. The present study is, therefore, organised broadly into three parts, namely, characterisation of aerosol properties using the ground-based MWR, validation of satellite products with the ground-based observations to improve further the MODIS algorithm and investigation of aerosol transport and their influence on aerosol radiative forcing.

2 Description of the experimental site

The present experimental site, Mohal (31.9°N, 77.12°E, 1154 m amsl), is located in the Kullu valley of the northwestern part of the Indian Himalayas (Fig. 1). The famous River Beas flows in the middle of Kullu valley. The Kullu valley, extending up to 80 km long from south to north and is 2 km wide, begins from Larji (957 m amsl) in the lower Beas basin and stretches up to the Rohtang Crest (4,038 m amsl) in the upper Beas basin (Kuniyal et al. 2009). The Mohal is a gentle flat region lying in the middle of the Kullu valley, which is a soap-dish type of shape and is surrounded by mountains of considerable height in the range 3,000–5,000 m. The lower part of the Kullu valley starting from Aut in the south to Katrain in the north falls under the rain shadow zone and receives snowfall in winter on adjoining hills (Sharma et al. 2009). However, the observation site remains far away from the snow line. Due to rapidly growing urbanisation in the recent years, the surrounding environment in the immediate vicinity of the experimental site is dominated by tourism and agro-horticultural activities

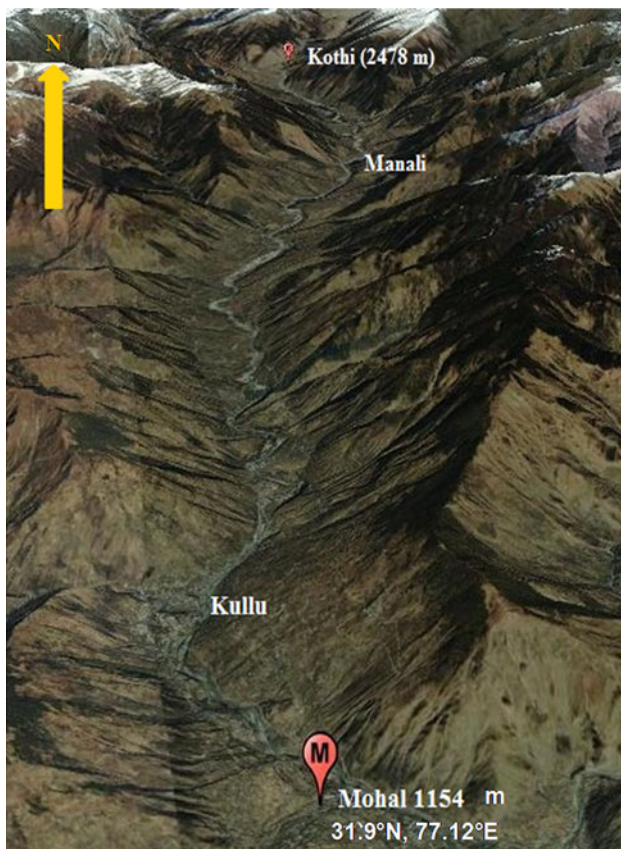


Fig. 1 View of the Kullu valley (source: Google Earth)

(Kuniyal et al. 2007), and is characterised with semi-urban settlement (by converting arable land into house constructions for dwelling) (Kuniyal et al. 2007). Nowadays, this part of the Indian Himalayas has attracted a significant scientific interest due to the transport of ever-increasing anthropogenic aerosols from the Indo-Gangetic Plain (IGP) and natural aerosols from the Thar Desert to the Himalayas, and their resultant adverse impact on glaciers (Gautam et al. 2009; Prasad et al. 2009). Figure 2 shows the monthly mean prevailing synoptic wind vectors drawn at 700 hPa obtained from the National Centers for Environment Prediction (NCEP) reanalysis website (<http://www.cdc.noaa.gov/cgi-bin/data/composites/printpage.pl>). A persistent north-westerly air mass flows with high intensity in the northern part of India. The wind vectors confirm the dispersion of anthropogenic aerosols from the IGP and desert aerosols from the Thar Desert to the Indian Himalayas.

3 Instrumentation, data and analysis

3.1 Ground-based measurements

The ground-based AOD measurements are carried out by using the MWR at Mohal from January 2007 to December

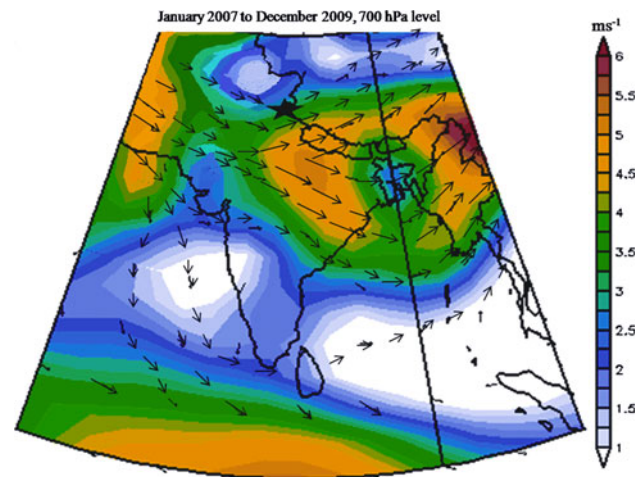


Fig. 2 The monthly mean climatological wind patterns at 700 hPa over the Indian region. The *shades* represent the magnitudes of wind in ms^{-1} , the *arrows* show direction and the *star* denotes the location of the Kullu valley

2009. These measurements are carried out under clear sky conditions when no visible clouds appear around the solar disc. During the observation period, the prevailing weather conditions remained unfavourable most of the days in terms of clear sky conditions. This limited the ground-based AOD measurements and it remained the main factor for the irregular distribution of the observational days. From a viewpoint of the daily distribution of AOD, there are only 163 days when measurements during the forenoon (FN) and afternoon (AN) parts of the day became possible. The AOD measurements during June and July 2008, May and August 2009 have not been possible due to unfavourable clear sky conditions. The ground-based MWR was designed and developed at Space Physics Laboratory, Thiruvananthapuram, following the principle of filter wheel radiometer (Shaw et al. 1973; Moorthy et al. 1999). The MWR measures the spectral extinction of surface direct solar flux at ten wavelengths, centred at 380, 400, 450, 500, 600, 650, 750, 850, 935 and 1,025 nm, with the full width half maximum band at the range of 6–10 nm at different wavelengths as a function of the solar zenith angle (SZA). The radiation passes through a field of view (FOV) limited to 2° using lens pin-hole detector optics, so that the effect of diffuse radiation entering into the FOV on the retrieved optical depths may be insignificant (Moorthy et al. 1998). The instrument is semi-automatic in nature. Before tracking the sun, the optical unit is mechanically adjusted on an equatorial mount and allowed to move at every 12 s around the orthogonal axis with an angular speed equal to 0.05° in order to keep the MWR always aligned towards the sun. The raw data obtained through the MWR are analysed following the Langley technique to deduce the total columnar optical depth

(Shaw et al. 1973; Moorthy et al. 1991; Gogoi et al. 2008, 2009). In analysing the MWR data, the data collected during FN and AN parts of the day are averaged so as to be considered as a single data set. The attenuation of solar radiation along the slant path depends on the scattering and absorption of radiation as described by the Lambert–Beer law:

$$E_{\lambda} = E_{o\lambda} \exp(-m\tau) \quad (1)$$

where E_{λ} is the solar radiation incident at the surface, $E_{o\lambda}$ is the solar radiation incident at the top of the atmosphere, m is the relative air-mass as a function of SZA $\leq 70^{\circ}$ and τ is the total columnar optical depth that stands for different atmospheric extinction processes, i.e. scattering by air molecules ($\tau_{r\lambda}$), aerosols ($\tau_{p\lambda}$) and due to gaseous absorption ($\tau_{\alpha\lambda}$) (Moorthy et al. 1991), which is explained as follows:

$$\tau = \tau_{r\lambda} + \tau_{\alpha\lambda} + \tau_{p\lambda} \quad (2)$$

In the logarithm scale, Eq. 1 yields a straight-line equation:

$$\ln E_{\lambda} = \ln E_{o\lambda} - m\tau \quad (3)$$

Therefore, a plot of $\ln E_{\lambda}$ versus m , i.e. Langley plot, yields a straight line of slope $-\tau$ (Moorthy et al. 1999). The spectral AOD is derived for each observation day by using Eq. 2 (Moorthy et al. 1996):

$$\tau_{p\lambda} = \tau - (\tau_{r\lambda} + \tau_{\alpha\lambda}) \quad (4)$$

3.1.1 Major uncertainties of Multi-wavelength

Radiometer calibration coefficients in the derivation of aerosol optical depth

The accuracy of the retrieved AOD depends mainly on the accuracy of the calibration coefficients from ground-based MWR measurements. This section describes the major uncertainties of calibration coefficients arising during processing of the data. The stability of the Langley intercept, i.e. $\ln E_{o\lambda}$, also called the zero air-mass intercept, corrected for the daily variation of the sun–Earth distance is used as an indirect calibration of the instrument. Since the Langley intercept remains invariant over many years, any change in the zero air-mass intercept arises from variations in the MWR calibration coefficients. During the study period, the stability of the instrument observed to be fairly good, with the Langley intercept within 7% of the mean for the worst cases at 500 nm wavelength. The fluctuations were found to be relatively higher at $\lambda < 500$ nm compared to those at $\lambda > 500$ nm. A few days during which significant deviation was observed were not taken for further analysis. The overall error in the derivation of AOD using the Langley technique is explained as follows (Russell et al. 1993):

$$\begin{aligned} \delta\tau_{p\lambda} = & [\tau_{p\lambda}(\delta F/F)]^2 + [\tau_{\lambda}(\delta m/m)]^2 + [1/m(\delta E_{o\lambda}/E_{o\lambda})]^2 \\ & + [1/m(\delta E_{\lambda}/E_{\lambda})]^2 + [\Delta\tau_{i\lambda}]^2 \end{aligned} \quad (5)$$

The first term on the right-hand side of the above equation represents the error arising due to diffused scatter radiation; the second term is the error arising due to 1-s resolution in time for the air-mass calculation; the third term represents the error arising due to uncertainty of the Langley intercept calibration output; and the fourth term represents the error arising due to uncertainty in the MWR output. These errors contribute to <0.02 . The fifth term ($\Delta\tau_{i\lambda}^2 = \delta\tau_{r\lambda}^2 + \delta\tau_{\alpha\lambda}^2$) represents the total error arising in the estimation of the optical depth by molecular scattering and absorption, which contribute to <0.01 . The AOD may, therefore, have a maximum uncertainty of 0.03. For the detailed analysis of the MWR data and the error involved in it, see also Moorthy et al. (1999), Sagar et al. (2004), Saha et al. (2005) and Gogoi et al. (2008).

3.1.2 Determination of Ångström parameters

The use of the Ångström exponent (α) has significantly increased in the last several years because this parameter is easily estimated using an automated-surface sun radiometer and is also accessible to satellite retrievals (Schuster et al. 2006). The values of $\alpha \leq 1$ indicates a size distribution dominated by coarse mode size aerosols ($r \geq 0.5 \mu\text{m}$) that are typically associated with dust and sea salt (Eck et al. 1999; Schuster et al. 2006). The values of $\alpha \geq 2$ indicates a size distribution dominated by fine mode size aerosols ($r \leq 0.5 \mu\text{m}$) that are usually associated with urban pollution and biomass burning (Eck et al. 1999; Schuster et al. 2006). The spectral AOD is related to α and β by the Ångström Power Law (Ångström 1961) as follows:

$$\tau_{p\lambda} = \beta \lambda^{-\alpha} \quad (6)$$

where λ is expressed in μm . The Ångström Power Law is a special case of a more complicated equation valid for a limited range of particle diameters and limited interval of wavelengths. The logarithm scale of Eq. 6 yields a straight-line equation:

$$\ln \tau_{p\lambda} = \ln \beta - \alpha \ln \lambda \quad (7)$$

α and β were computed for an individual data set in the wavelength range 0.38–1.025 μm using Eq. 7 by evolving a linear least square fit between $\ln \tau_{p\lambda}$ versus $\ln \lambda$. Therefore, $\ln \tau_{p\lambda}$ versus $\ln \lambda$ yields a straight line of slope $-\alpha$ and intercept $\ln \beta$ (Ganesh et al. 2005). The optical depth measured at wavelength 0.935 μm is not included in the α and β calculations due to a strong water vapour absorption band; about 75–90% of the measured optical depth at this

wavelength is due to atmospheric water vapour (Moorthy et al. 1991).

3.2 Satellite measurements

3.2.1 MODIS data

The first measurements of aerosols over land through the use of satellite remote sensors became possible after the launch of POLDER, POLarization and Directionality of the Earth's Reflectances (Deschamps et al. 1994; Kaufman et al. 2002). It lasted for only 8 months due to technical problems in the spacecraft. Aerosol monitoring over land entered a new era with the launch of the MODIS instrument on board of the Terra and Aqua satellites. MODIS is a space borne remote sensor which imparts information about the global distribution of aerosols and their properties (Yu et al. 2004; Remer et al. 2005). MODIS acquires daily global data in 36 spectral bands from visible to thermal infrared spectral bands. The spatial resolution of these spectral bands (pixel size at nadir) is 1,000, 500 and 250 m with 29, 5 and 2 spectral bands, respectively. These satellites have been providing data since February 2000 and July 2002, respectively. Terra and Aqua operate at an altitude of 705 km, with an equatorial crossing time at 10:30 Indian Standard Time (IST) ascending towards the north and at 13:30 IST descending towards south, respectively (Yu et al. 2004; Remer et al. 2005; Levy et al. 2007).

In the present study, daily MODIS level 2 AOD data obtained from MOD04_L2 (data collected from the Terra platform) and MYD04_L2 (data collected from the Aqua platform) products are used. MODIS at 550 nm have a spatial resolution of 500 m. This results in 20×20 -pixel boxes for 10×10 -km resolution. The geolocation of each output pixel is computed from the aggregation of 10×10 boxes of L1B 1-km input, taking the average of the four central (column, row) pairs, such as: (5,5), (5,6), (6,5), (6,6) 1-km L1B input pixels. The data collected from the Terra and Aqua satellites as a representative of FN and AN parts of the day, respectively, are averaged in order to be considered as a single data set. Similar techniques to mix data sets are also adopted by Aloysius et al. (2008) and Kedia and Ramachandran (2008) to obtain the daily mean AOD. Remer et al. (2005) confirmed that the AOD values retrieved from MODIS are accurate within an uncertainty limit of $\Delta\tau_{p\lambda} = \pm 0.05 \pm 0.15\tau_{p\lambda}$ over the land, where $\tau_{p\lambda}$ is the ground-based AOD value. To compare the daily mean AOD from ground-based and satellite observations at the same wavelength, the data sets of MODIS AOD are sorted according to the MWR AOD. To recover the error occurred due to differences in wavelength dependence, the linear interpolation technique is used to calculate the AOD

value at 550 nm using the Power Law (Prasad et al. 2007) as:

$$\text{AOD}_{550\text{nm}} = \text{AOD}_{500\text{nm}}(550/500)^{-\alpha} \quad (8)$$

where α obtained in the visible spectrum lies in the range 400–750 nm.

The deviation between the ground-based and satellite observations is examined through root mean square deviation (RMSD) and mean absolute bias deviation (MABD) using equations given by:

$$\text{RMSD} = \sqrt{\left(\sum d_i^2/N_{\text{obs}}\right)} \quad (9)$$

and:

$$\text{MABD} = \sum |d_i|/N_{\text{obs}} \quad (10)$$

The other statistical measures used in the study are the correlation coefficient (r), standard deviation ($\pm\sigma$) and relative difference (RD), which are expressed as:

$$r = \frac{\left[\sum (x - \bar{x})(y - \bar{y})\right]}{\sqrt{\left[\sum (x - \bar{x})^2\right]\left[\sum (y - \bar{y})^2\right]}} \quad (11)$$

$$\pm\sigma = \sqrt{\left[\sum (x - \bar{x})^2/(N_{\text{obs}} - 1)\right]} \quad (12)$$

and:

$$\text{RD} = (|d_i|/\tau_{\text{MWR}}) \times 100 \quad (13)$$

In Eqs. 9–13, d_i is the difference between the MWR and MODIS-derived AOD, N_{obs} is the number of data pairs, and x and y are the mean sample of series X and Y , respectively.

3.2.2 CALIPSO data

Cloud Aerosol Lidar and Infrared Pathfinder Satellite Observations (CALIPSO) is a part of the A-Train constellation of satellites and have been making global measurement of aerosols and clouds since 13 June 2006. The main objective of CALIPSO is to study the impact of clouds and aerosols on the Earth's radiation budget and climate. Unlike the space-based passive remote-sensing instruments, CALIPSO can observe aerosols over bright surfaces and beneath thin clouds, as well as with clear sky conditions (Huang et al. 2008). Using depolarisation techniques, CALIPSO can easily distinguish dust from other types of aerosols (Liu et al. 2008). The CALIPSO satellite comprises three instruments: the Cloud–Aerosol Lidar with Orthogonal Polarization (CALIOP), the Imaging Infrared Radiometer (IIR) and the Wide Field Camera (WFC). CALIPSO Lidar is designed to acquire vertical profiles of elastic backscatter at two wavelengths (532 and 1,064 nm) from a near-nadir viewing geometry during both

day and night phases of the sun-synchronous orbit. CALIPSO has a 98° inclination orbit and flies at an altitude of 705 km, providing daily global maps of the vertical distribution of aerosols and clouds. The CALIPSO Lidar Level 1 (version 3.01) consisting of optical and physical properties of the detected aerosol layers is used in the present study. For more detail, see Powell et al. (2009).

3.3 Air back trajectory

In order to examine the transport of aerosols from remote sources to the studied region, 5-day air back trajectories are plotted using the HYbrid Single-Particle Lagrangian Integrated Trajectory (HYSPLIT) model. Global Data Assimilation System (GDAS) meteorological data is used to run the HYSPLIT model with the latitude–longitude grid (Draxler and Rolph 2010). The air trajectories are calculated for 11:30 IST at three arrival heights: 1,500, 2,500 and 4,000 m above ground level (AGL). The experimental site is surrounded by mountains whose tops range between 3,000 and 5,000 m (Sharma et al. 2009). The selections of all level trajectories are made keeping in mind the valley topography, mountain peaks and boundary layer over Mohal.

3.4 Computation of aerosol radiative forcing

The aerosol radiative forcing at the top of the atmosphere (TOA) and at the surface (SFC) is defined as the difference in the net fluxes with and without aerosol at the TOA and at the SFC, respectively (Satheesh et al. 2002). Aerosol radiative forcing (ΔF) at TOA and SFC can be expressed as (Kedia et al. 2010):

$$\Delta F_{\text{TOA, SFC}} = \text{flux}(F^\downarrow - F^\uparrow)_{\text{withaerosolTOA,SFC}} - \text{flux}(F^\downarrow - F^\uparrow)_{\text{withoutaerosolTOA,SFC}} \quad (14)$$

In the present study, the net flux is computed in the wavelength range $0.175 \mu\text{m} \leq \lambda \leq 4.0 \mu\text{m}$ with and without aerosols at the TOA and at the SFC using the radiation transfer model developed by Fu and Liou (1992, 1993). It is a delta-four stream radiative transfer scheme (Huang et al. 2009). Before running this radiation transfer model, it is essential to estimate a few parameters, such as AOD at 500 nm, surface albedo, cosine of zenith angle, surface elevation and the type of environment. The types of environment are model based defined by the International Geosphere Biosphere Programme. The surface albedo is the ratio of radiation reflected from a surface to the radiation incident on the surface and one can easily assess its values from Modern Era Retrospective-analysis for Research and Applications (MERRA). MERRA is a reanalysis for the satellite era produced in the National Aeronautics and Space

Administration (NASA) Goddard Earth Observing System version 5 (GEOS-5) data assimilation model (Rienecker et al. 2008). The analysis is performed at a horizontal resolution of $2/3^\circ$ longitude by $1/2^\circ$ latitude and 72 levels (top at 0.01 hPa). The data presented here can be obtained from using the NASA GIOVANNI web-based application (<http://disc.sci.gsfc.nasa.gov/giovanni>). The cosine of zenith angle describes the position of the sun relative to a location on Earth and can be estimated from the equation described by Iqbal (1983).

The difference between the radiative forcing at the TOA and SFC is defined as the atmospheric forcing (ΔF_{ATM}) and is written as (Kedia et al. 2010):

$$\Delta F_{\text{ATM}} = \Delta F_{\text{TOA}} - \Delta F_{\text{SFC}} \quad (15)$$

The ΔF_{ATM} represents the amount of energy trapped within the atmosphere due to the presence of aerosol. Thus, the heating experienced by the atmospheric layer due to radiation transfer is expressed in terms of the rate of temperature changes and is calculated from the First Law of Thermodynamics together with hydrostatic equilibrium (Liou 2002; Babu et al. 2007; Kedia et al. 2010):

$$\partial T / \partial t = g / C_p (\Delta F_{\text{ATM}} / \Delta P) \times 24 \times 3600 \quad (16)$$

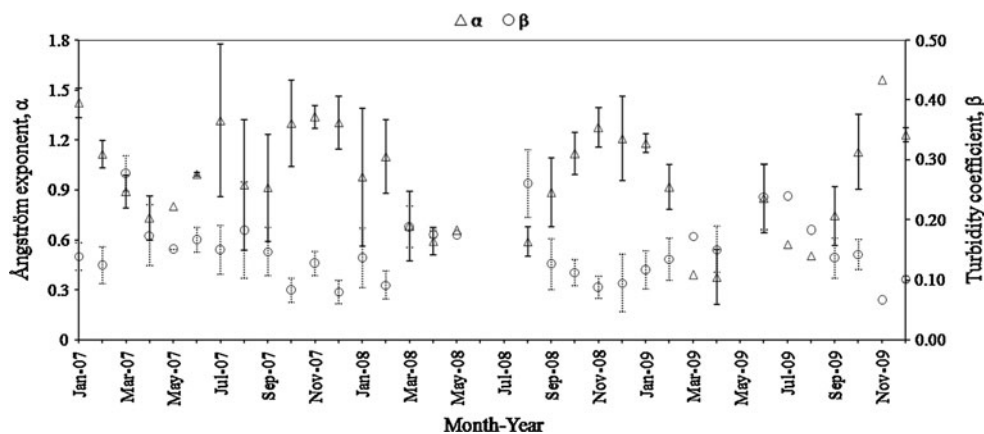
where $\partial T / \partial t$ is the heating rate in K day^{-1} , g / C_p is the lapse rate (taking g as the acceleration due to gravity and C_p as the specific heat capacity of air at constant pressure = $1,006 \text{ J kg}^{-1} \text{ K}^{-1}$) and ΔP is the atmospheric pressure difference (taking ΔP as 300 hPa, mid-latitude pressure width of troposphere), meaning that the aerosol layer is concentrated in the first 3 km above ground (Ramanathan et al. 2001; Prasad et al. 2007).

4 Results and discussion

4.1 Characteristics of aerosol optical depth

The AOD measurements are carried out over Mohal from January 2007 to December 2009. These measurements are conducted under clear sky conditions when no visible clouds appear around the solar disc. The daily average (mean \pm standard deviation) AOD at 500 nm ($\text{AOD}_{500\text{nm}}$) is found to be 0.24 ± 0.08 and ranges from 0.10 to 0.50. During 2007, 2008 and 2009, these values are found 0.23 ± 0.07 , 0.24 ± 0.07 and 0.28 ± 0.09 , respectively. In respect of seasonal variations, the highest $\text{AOD}_{500\text{nm}}$ is found to be 0.29 ± 0.08 in the pre-monsoon season (April–July) due to the high degree of human interference in the form of tourism and external dust transport from the country lying in the northwestern part of India. The pre-monsoon is followed by a value of 0.26 ± 0.07 in the monsoon season (August–September), 0.22 ± 0.07 in the

Fig. 3 Temporal variation in Ångström parameters, α and β



post-monsoon season (October–November) and 0.21 ± 0.06 in the winter (December–March).

4.2 Analysis of Ångström parameters

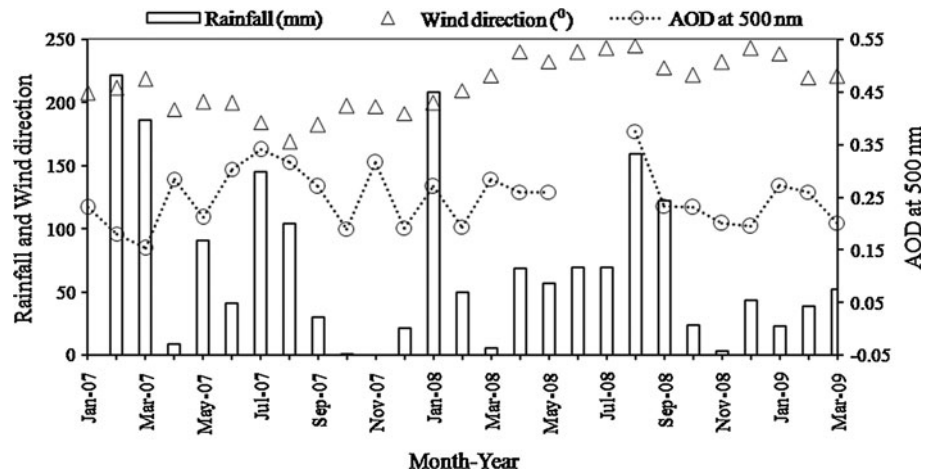
For retrieval of the aerosol size distribution and the total aerosol loading in the columnar environment, α and β are computed in the wavelength band 380–1,025 nm. The daily average values of α and β are obtained as 1.02 ± 0.34 and 0.13 ± 0.05 , respectively. The temporal variations among Ångström parameters are shown in Fig. 3. When α values increase, the β values decrease and vice versa. An inverse relationship is found between α and β , with considerable negative correlation around -0.64 . Figure 3 illustrates the relatively highest concentration of fine size aerosols in the winter and post-monsoon periods, while the lowest concentration was observed in the pre-monsoon and monsoon periods. During winter, the low MWR AOD_{500nm} values associated with $\alpha > 1.0$ indicates that the size distribution is dominated by anthropogenic aerosols (i.e. $r \leq 0.5 \mu\text{m}$), which are mostly attributed to biomass burning and frequent incidents of forest fire at local levels (Kuniyal et al. 2009). During this season, the degree of fuel wood burning in the valley reached its maximum level and here remained the main source of fine size aerosols. Thereafter, with the decrease in anthropogenic activities like burning fuel wood, coal etc., there was noticed a sharp reduction in fine size aerosols up to April. During the pre-monsoon period, high MWR AOD_{500 nm} values associated with $\alpha < 1.0$ indicates the size distribution dominated by dust aerosols (i.e. $r \geq 0.5 \mu\text{m}$), which are mostly transported from the Great Sahara and Thar Desert regions (Kuniyal et al. 2009). Back trajectory analysis in conjunction with MODIS and CALIPSO satellite data reveals that the frequency of dust storm and dust aerosol transport increases after March from the western deserts. The similar results of dust aerosol transport from the western deserts towards the Himalayan-Gangetic region have also been reported (Middleton 1986; Prospero et al. 2002; Singh et al. 2004; Gautam et al. 2009). As a result,

long-range transport caused a sharp increase in coarse size particles, which are noticed after March, and these dust transport events continued up to June. On the other hand, there was noticed a continuous increase in α after April. The major reason for this is considered to be the high degree of human interference in the form of unregulated tourism (April–July) and their related activities to generate more fine size aerosols. After September, the influence of human interferences again starts to increase due to the International Kullu Dussehra festival, which, almost every year falls in October. After getting over Kullu Dussehra, the festival's influence minimises, but, due to the onset of winter fuel wood burning for cooking and heating purposes, it increases, as a result of which, fine size aerosol increases and/or remains almost constant from October to December.

4.3 Effect of prevailing wind and precipitation on the characteristics of the aerosol optical depth

The climatological values of monthly total rainfall and observed prevailing wind direction along with the AOD measured at 500 nm is plotted in Fig. 4. The data of climatological values are acquired from the Automatic Weather Station installed at Mohal. Due to some technical reasons, the availability of data after March 2009 was not possible. Figure 4 shows that the maximum rainfall occurs in February 2007 and January 2008. The synoptic winds over Mohal show that the dominant wind sector is south-southwest, contributing 62%. However, the contribution of the southwest-west wind sector is also significant, contributing 33%. In general, south-westerly winds confirm the dispersion of anthropogenic aerosols from the plains of India and dust aerosols from the western deserts towards Mohal. Figure 2 illustrates the vertical velocity (shaded region) and horizontal wind at the 700-hPa level. Distinct descent motion of about 2 ms^{-1} is noticed over southern India and ascent motion stronger than 4.5 ms^{-1} appears over northern India. The upward velocity of about 3 ms^{-1} is noticed over the Kullu valley, which is driven by the sensible heat flux caused

Fig. 4 Temporal variation in the aerosol optical depth (AOD) at 500 nm, rainfall and wind direction



by the radiative heating on the surface. Examining the characteristics of AOD at 500 nm in the light of Fig. 4 suggests that, during January 2007, the AOD value was 0.23 and precipitation was negligible. During February–March 2007, Mohal received intense rainfall and the AOD decreased by 35%. In April 2007, dust events start to increase, a little bit of rain is not able to maintain the wet removal process and the AOD abruptly increases by 87%. May–June 2007 remains as having dust storm occurring days, while July–August 2007 have the maximum contamination of cirrus clouds. This may be one of the reasons for the high AOD value. The peak in the AOD during November 2007 is due to dry weather. From November 2007 to February 2008, the AOD value fell by 41% due to the wet removal process. In March 2008, the valley almost went dry and there accumulated 47% aerosols in the atmosphere compared to February 2008. The rainfall intensifies from April 2008 and heavy rainfall occurred during August–September 2008. Due to adverse weather conditions, observations during June–July 2008 are not possible. The presence of cirrus type of clouds contamination may be one of the reasons for the high AOD values during August 2008. During October–November 2008, a little bit of rain brings no changes in the existing aerosol concentrations. About a 13% increase in rain brings about a 3% decrease in the AOD in December 2008 compared to November 2008. On comparing February and March 2009, the month of March received 35% more rain and this reduced the aerosol concentrations by 23%. From the above discussion, it is known that, while studying the characteristics of AOD, one cannot ignore the influence of meteorological factors.

4.4 Comparison of the aerosol optical depth from ground and satellite observations

Figure 5a represents the scatter plot of AOD_{550nm} between MODIS and MWR observations. The data are sorted

according to the MWR AOD. The dashed line is the 1:1 line and the error bars denote the expected accuracy calculated from prelaunch analysis over land ($\Delta\tau_{p\lambda} = \pm 0.05 \pm 0.15\tau_{p\lambda}$) (Remer et al. 2005). The percentage retrieval for daily AOD_{550nm} over Mohal within the expected accuracy is estimated to be 87%, with a significant correlation coefficient of 0.76, whereas Remer et al. (2005) reported the expected accuracy with respect to AERONET-derived AOD_{550nm} over the Indian land area to be around 90%. The percentage error between MODIS retrieval and MWR observations at 550 nm is 5%, showing a systematic bias in which the MODIS AOD is underestimated by the MWR AOD. It is obvious from Fig. 5a that the MODIS AOD retrieval has a good correlation with MWR measurements. The scattered plot (see Fig. 5a) of ground-based AOD measurement with the corresponding values are derived from MODIS and shows a good agreement with RMSD, MABD and correlation coefficients of 0.05, 0.04 and 0.76 for daily observations, respectively. These agreements enabled us to validate the satellite data. However, MODIS seems to underestimate its AOD compared to the MWR AOD; the regressed slope was 0.82 for daily observations. The deviation of the slopes from the unity of correction line 1:1 indicates a systematic bias, which could be caused due to error in instrument calibration and/or inappropriate choice of the aerosol model in the MODIS retrieval algorithm and some other factors (Chu et al. 2002; Zhao et al. 2002; Remer et al. 2005).

Figure 5b, c shows the monthly mean and seasonal mean AOD_{550nm} values retrieved from MODIS and MWR over Mohal during 2007–2009. It can be seen from Fig. 5b, c that, for each month and season, MODIS AOD are mostly matched with the corresponding MWR values. But the MODIS AOD values are relatively lower than the MWR values, except for a few months. The monthly mean and seasonal mean AOD shows very similar variations. The absolute difference found between the monthly mean

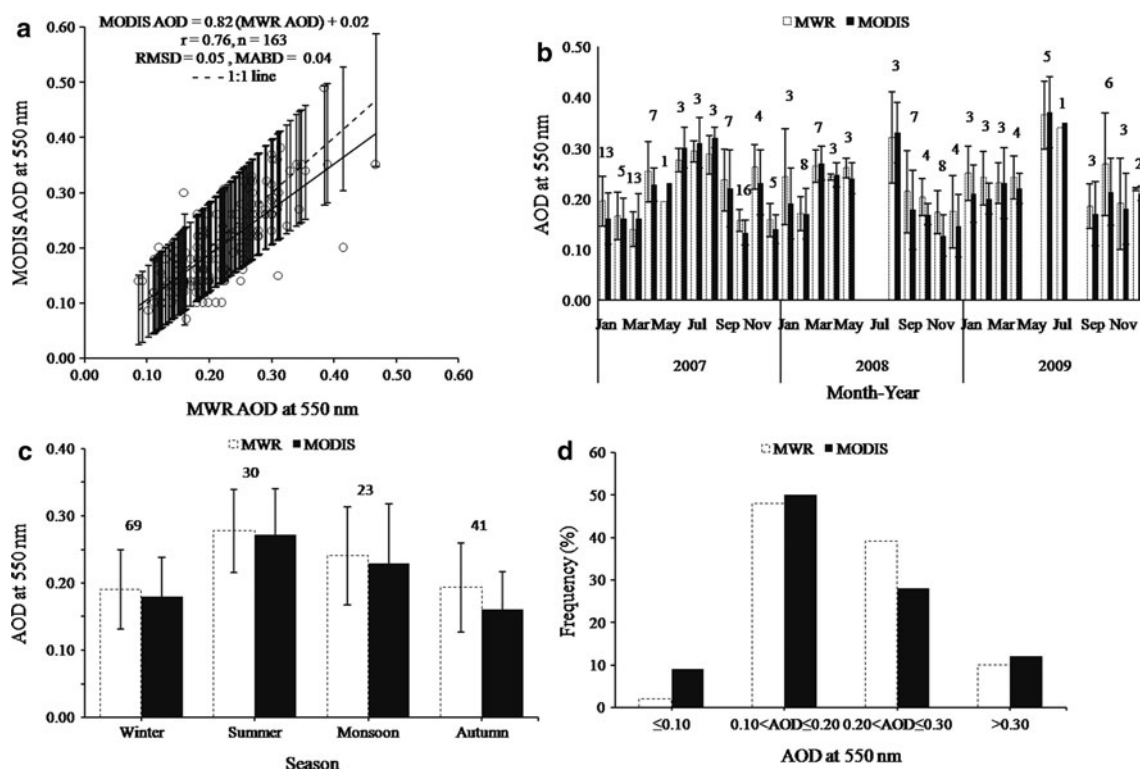


Fig. 5 a Scatter plot between AOD derived from Moderate Resolution Imaging Spectroradiometer (MODIS) and Multi-wavelength Radiometer (MWR). The error bars indicate the range of MODIS expected accuracy ($\Delta\tau_{p\lambda} = \pm 0.05 \pm 0.15\tau_{p\lambda}$) from the 1:1 line. b, c Variations in monthly and seasonal average AOD retrieved from

MODIS and MWR. The error bars represent the standard deviation of the AOD. The numbers above the histograms of MODIS and MWR represent the number of data points for the respective month and season. d Frequency distribution of AOD derived from MODIS and MWR

MODIS AOD and the MWR AOD is 0.01. As the international Kullu Dussehra festival approaches, the anthropogenic activities such as vehicle interference, burning of fuel wood etc. start to increase before the onset of this period and reaches its peak in October, whose impact remains continued for a month or more. The high AOD retrieved through MWR during September–January is considered due to local as well as external sources. This study suggests that, during September–January in the Mohal region, the aerosol types are polluted dust and smoke produced from biomass burning. From the MODIS airborne simulator data acquired over Brazil, during Smoke Carbon Aerosol and Radiation-Brazil (SCAR-B), it is found that, over smoke aerosol regions, the value of single scattering albedo (SSA) is very sensitive to the retrieved AOD (Chu et al. 1998). Ichoku et al. (2003) conducted ground-based observation on aerosol properties during the SAFARI 2000 experiment. The investigations mainly focused on the behaviour of MODIS aerosol product, especially in regard to the smoke aerosol produced due to biomass burning. Their study observed that, during the biomass burning period, the AOD values predicted by MODIS are relatively lower than ground-based observation, since the SSA for biomass burning aerosol is

significantly lower, which, in turn, reduces the surface albedo. Myhre et al. (2005) reported a significant reduction in the surface albedo in fire-prone areas over the African continent typically in the ranges of 5–8%. Over Mohal, the intercept estimate is close to 0.1, which implies a small amount of over-correction for the surface reflectance in the MODIS channel at 550 nm (Misra et al. 2008). In light of the above results, this study reveals that the assumption of the surface reflectance in the MODIS aerosol model is overestimated, which results in an underestimation of the MODIS AOD. Hence, to recover the systematic bias, the existing retrieval algorithm needs to be modified in view of the changing aerosol optical properties, especially during the biomass burning period (September–January).

The frequency distribution of AOD values from the data points of MODIS and MWR are presented in Fig. 5d. From this figure, it is made clear that the majority of AOD values is between $0.10 < AOD \leq 0.20$, where the frequency difference is around 2%. The frequency distribution of $AOD \leq 0.10$ is considerably (7%) higher for MODIS than that of MWR. In the AOD range > 0.30 , the frequencies of the MODIS AOD are approximately correspondent with those of the MWR AOD. The frequency distribution patterns shown in Fig. 5d suggests the underestimation of the

MODIS AOD in the range $0.10 < \text{AOD} \leq 0.30$ with respect to the MWR. This study indicates that MODIS AOD retrievals are able to effectively characterise the AOD distribution over Mohal, but further efforts to eliminate systematic errors in the existing MODIS algorithm are needed.

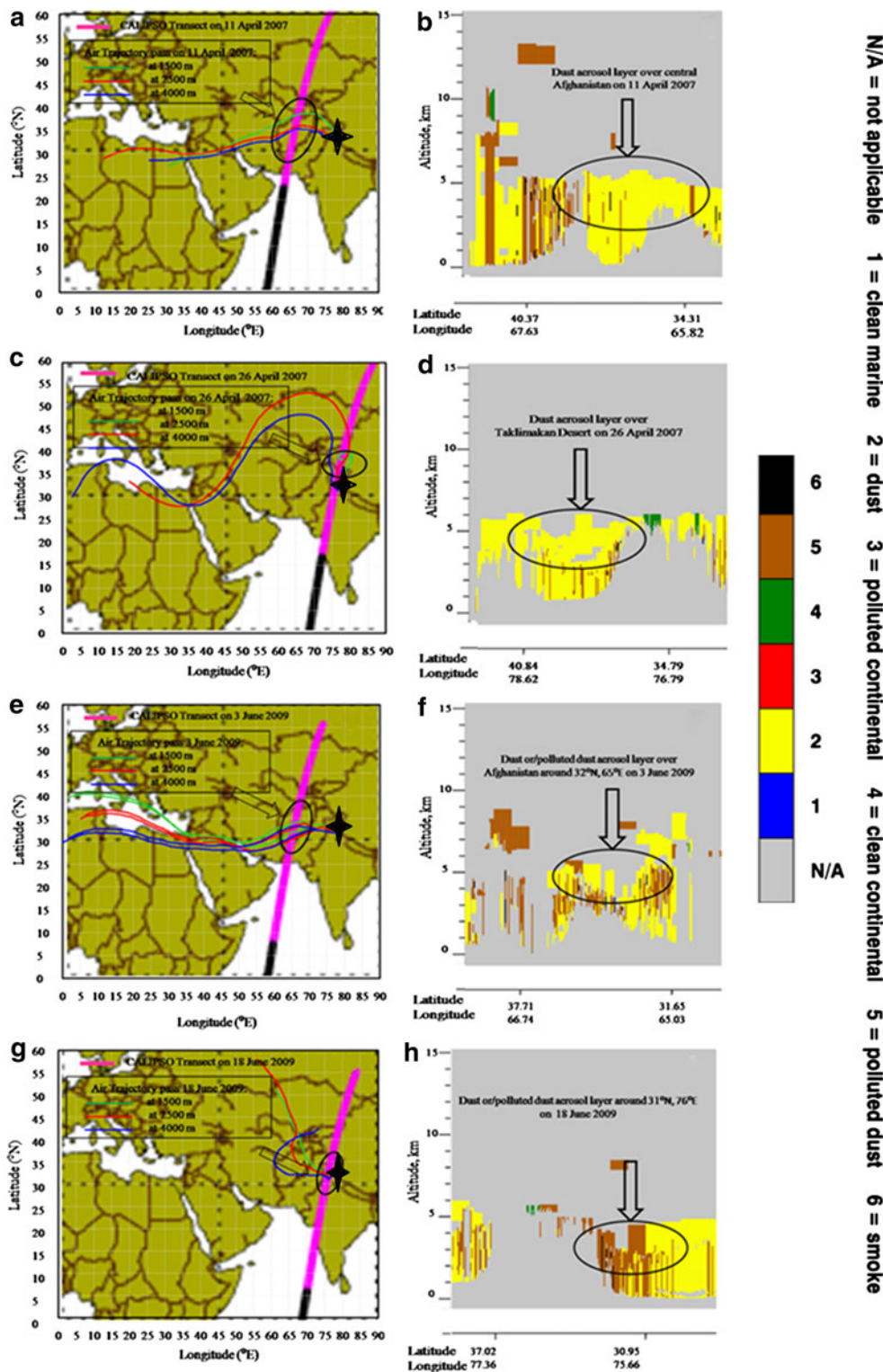
4.5 Investigation of aerosol transport

To investigate the influence of long-range transport from different sources of origin to Mohal in the northwestern Indian Himalaya, besides local sources contributing to the existing columnar aerosols, external sources are also identified. The study of aerosol transport towards Mohal is investigated on some characteristic cases with the simultaneous study of back trajectory in conjunction with CALIPSO. The results of the studies suggest that the external desert and anthropogenic aerosols reached Mohal. Kuniyal et al. (2009) also investigated the aerosol origin by taking into account back trajectories analysis. That study indicated that, during the pre-monsoon period, the AOD at Mohal was largely influenced due to the Sahara aerosols. The various studies showed that the dust storm started in April and remained until the end of June. These dust storms remain associated with the westerly flow and play a major role in building the aerosol layer, which is an effective dust source for the Indian sub-continent (Dey et al. 2004; Bollasina and Nigam 2009). The depolarisation ratio is defined as the ratio of the perpendicular and the parallel components of the attenuated backscatter signal, and is a good proxy to distinguish different dust aerosols. Higher depolarisation suggests the presence of large concentrations of dust particles in the layer in cloud-free conditions (Gautam et al. 2009). The air parcels suggest the transport of dust aerosols towards Mohal from a desert-prone region. The CALIPSO-derived image is used to identify the dust aerosols along the overpass of the trajectory. Typical examples of the highest value of AOD noticed over Mohal during the dust storm period (April–June) are taken under consideration.

During dust storm period of 2007, the highest peak of MWR $\text{AOD}_{500\text{nm}}$ is obtained on 12 April (MWR $\text{AOD}_{500\text{nm}} = 0.34$), followed by 27 April, as well as on 1 June (MWR $\text{AOD}_{500\text{nm}} = 0.33$), while the lowest peak is observed on 21 April (MWR $\text{AOD}_{500\text{nm}} = 0.18$). The air parcels reached on 12 April over Mohal originated from the Sahara Desert and those passed through the Libyan Desert and the Syrian Desert (Fig. 6a). Due to westerly flow, these air parcels passed through Afghanistan and played a major role in building the aerosol layer over Afghanistan. The nearest CALIPSO pass was available on 11 April in the nighttime, transecting across Afghanistan. Figure 6b is the CALIPSO-derived image, taken on 11 April covering

the central Afghanistan region, depicting a vertically extended dust aerosol layer of 5 km. The higher depolarisation ratio (i.e. 0.4) profile derived from CALIOP backscatter measurements indicates that the desert dust lifting is associated with the near-surface aerosols. This aerosol transport has enhanced the dust aerosol loading on 12 April over Mohal. The air parcels reached on 27 April over Mohal originated from the Sahara Desert (plot at 2,500 and 4,000 m) and Taklimakan Desert (plot at 1,500 m) (Fig. 6c). The air parcels which originated from the Sahara Desert finally passed through the Taklimakan Desert. The Taklimakan Desert in Central Asia is one of the largest sandy deserts in the world and is a significant source of airborne dust (Huang et al. 2007; Liu et al. 2008). Heavy dust storms are mostly experienced during the pre-monsoon period and their impact over the Taklimakan Desert remains up to a few days after its occurrence (Huang et al. 2007). A dust storm which occurred on 22 April at the Taklimakan Desert had affected the present experimental site of Mohal. Figure 6d is the CALIPSO-derived image transecting across Taklimakan Desert on 26 April, depicting a vertically extended dust aerosol layer of 5 km. The higher depolarisation ratio of ~ 0.4 indicates that the desert dust lifting is associated with the near-surface aerosols. At the same time, air parcels also passed through this region, which proves that transport dust reached the present study region. In order to investigate the cause of high aerosol loading on 1 June over Mohal, it came to knowledge that, on 1 June, the entire trajectories reached Mohal through Afghanistan. These trajectories passed through Afghanistan on 31 May. The nearest CALIPSO pass was available on 31 May, showing a vertical dust aerosol layer of 5.3 km over Afghanistan between $32\text{--}37^\circ\text{N}$ and $68\text{--}70^\circ\text{E}$. The higher depolarisation ratio value of around 0.4 indicates that the desert dust lifted to elevated altitudes in the troposphere. During the dust storm period in 2009, the highest peak of MWR $\text{AOD}_{500\text{nm}}$ is obtained on 4 June (MWR $\text{AOD}_{500\text{nm}} = 0.50$), followed by 19 June (MWR $\text{AOD}_{500\text{nm}} = 0.42$), while the lowest peak is observed on 10 April (MWR $\text{AOD}_{500\text{nm}} = 0.13$). In order to investigate the possible sources of origin it came to knowledge that, on 4 June, the air parcels reached over Mohal originated from or passed through the Sahara Desert (Fig. 6e). Due to westerly flow, these air parcels moved towards Mohal. The nearest CALIPSO pass was available on 3 June in the nighttime, covering the region of Afghanistan. The CALIPSO-derived image covering the region of Afghanistan depicts a vertically extended dust or polluted dust aerosol layer of 5 km around 32°N , 65°E (Fig. 6f). This analysis has confirmed the dispersion of dust or polluted dust aerosols from the western deserts towards Mohal. The possible sources of aerosol transport on 19 June over Mohal are also analysed. Before reaching Mohal, these air

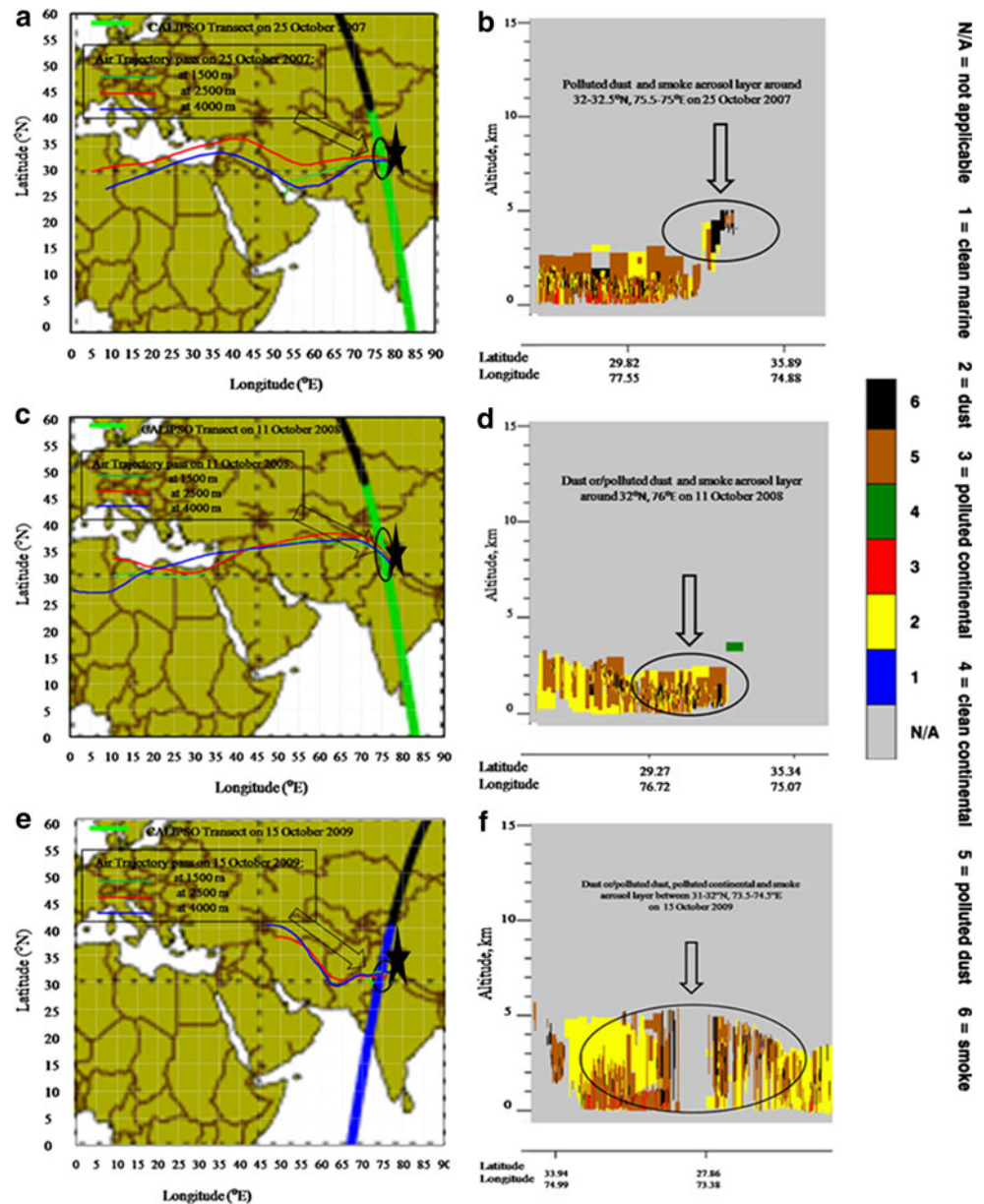
Fig. 6 Cloud Aerosol Lidar and Infrared Pathfinder Satellite Observations (CALIPSO)-derived image Lidar Level 1 (version 3.01) identifying the desert dust aerosols along the overpass trajectory. Typical examples to investigate the influence of long-range transport from different source origins to the Mohal during the dust storm period (April–June) are shown



parcels passed through 31°N, 76°E on 18 June (Fig. 6g). The CALIPSO-captured image over the pass time of air parcel suggests the indication of a vertically extended aerosol layer of dust or polluted dust around 31°N, 76°E (Fig. 6h).

The agricultural waste burning in the IGP and Punjab is a significant source of anthropogenic aerosols during October (Badarinath et al. 2009; Sharma et al. 2010). During October, air parcels suggest the transport of anthropogenic aerosols such as polluted dust, smoke etc.

Fig. 7 CALIPSO-derived image Lidar Level 1 (version 3.01) identifying the anthropogenic aerosols along the overpass trajectory. Typical examples to investigate the influence of long-range transport from different source origins to the Mohal during the biomass burning period (October) are shown



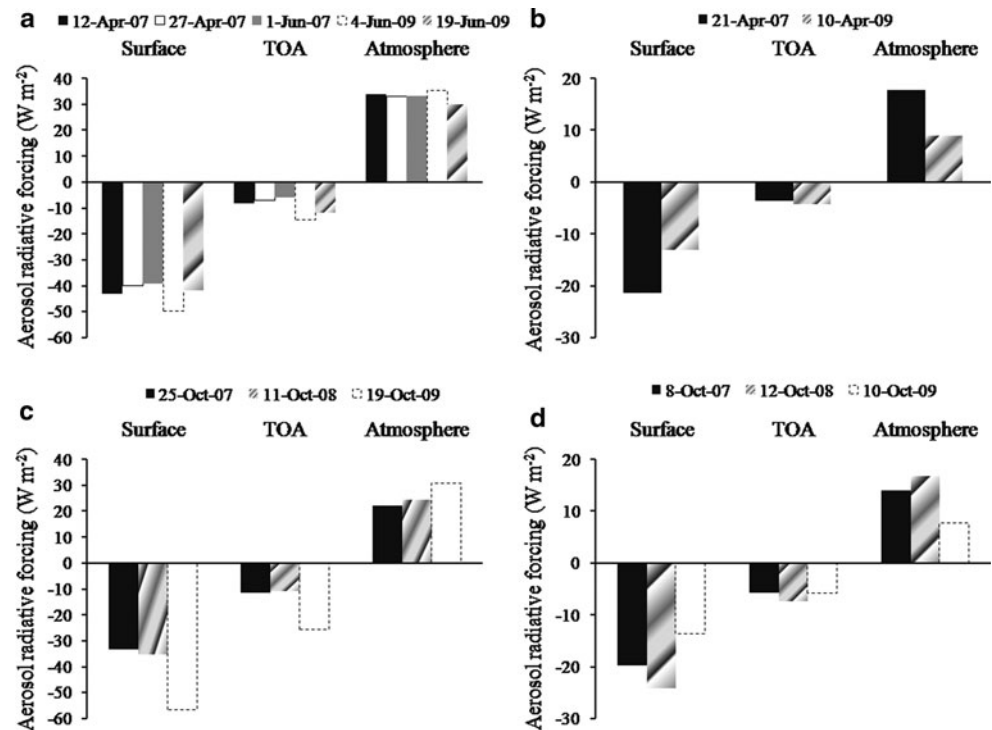
towards Mohal from a region that is dominated by agriculture crop residue burning. The CALIPSO-derived image is used to identify the smoke aerosols released from agriculture crop residue burning along the air trajectories. Typical examples of the highest value of AOD noticed over Mohal during October are taken into consideration.

During October 2007, Sharma et al. (2010) reported the highest peak of MWR-derived AOD_{500nm} over Patiala ($30.19^{\circ}N$, $76.4^{\circ}E$) on 25 October, followed by 31 October. These high values of AOD_{500nm} are attributed to the extensive burning of agricultural crop residues throughout Punjab. Similar results are also observed in our region. The air parcels reached over Mohal on 25 October passed through the northern part of Punjab (Fig. 7a). On 25 October, the nearest CALIPSO pass was available in the

daytime covering the northern part of Punjab, suggesting a vertically extended aerosol layer of polluted dust and smoke ~ 3 km around $32\text{--}32.5^{\circ}N$, $75.5\text{--}76^{\circ}E$, which is associated with burning agricultural crop residues (Fig. 7b). The AOD_{500nm} value was noted to be 60% higher on 25 October as compared to 8 October (lowest peak in AOD). About a 34% increase in the α estimate on 25 October when compared to 8 October suggests additional loading of fine aerosols in the atmosphere. There is a good agreement between AOD_{500nm} and α measured at Mohal and the values reported over Patiala (Sharma et al. 2010). These results indicate that the impact of agricultural crop residues burning over Punjab have an adverse impact over Mohal.

During October 2008, the highest peak of MWR AOD_{500nm} of 0.26 is obtained on 11 October, while lowest

Fig. 8 Aerosol radiative forcing estimates on: **a** desert dust aerosol transport days and result compared with **b** low aerosol loading days; **c** anthropogenic aerosol transport days and result compared with **d** low aerosol loading days



peak is obtained on 12 October. The movement of air parcels towards Mohal across the CALIPSO transect on 11 October (Fig. 7c). The CALIPSO-derived image taken on 11 October suggests a vertically extended aerosol layer (~ 3 km) of dust or polluted dust and smoke around 32°N , 76°E (Fig. 7d). This increased the possibility of the transport of anthropogenic aerosols towards Mohal. The $\text{AOD}_{500\text{nm}}$ value was noted to be 44% higher on 11 October when compared to 12 October. About a 23% increase in the α estimate on 11 October as compared to 12 October suggests the additional loading of fine aerosols in the atmosphere.

During October 2009, the highest peak of MWR $\text{AOD}_{500\text{nm}}$ of 0.47 is obtained on 19 October, while the lowest peak is obtained on 10 October. Figure 7e shows the movement of air parcels towards Mohal. The air parcel plot at 1,500 m originated from Pakistan around 29°N , 72°E . The nearest CALIPSO pass was available during nighttime on 15 October. The air parcel with slow motion within the boundary layer seems to follow the transect path of CALIPSO. The CALIPSO-derived image taken on 15 October suggested a vertically extended aerosol layer (~ 4 km) of dust or polluted dust, polluted continental and smoke between $31\text{--}32^{\circ}\text{N}$, $73.5\text{--}74.5^{\circ}\text{E}$ (Fig. 7f). This increased the possibility of aerosol transport towards Mohal. The $\text{AOD}_{500\text{nm}}$ value was noted to be 291% higher on 19 October when compared to 10 October. About a 350% increase in the α estimate on 19 October as compared

to 8 October suggests an additional loading of polluted aerosols in the atmosphere.

4.6 Influence of aerosol transport on aerosol radiative forcing

This section describes the radiative effect of aerosol over Mohal during desert dust transport days. Figure 8a–d shows the spatial distribution of short-wave aerosol radiative forcing at SFC, TOA and ATM. The results of the study are compared with low aerosol loading days. It can be seen from Fig. 8a that enhanced loading of desert dust aerosols from transport sources have a high impact, with a considerable reduction in surface-reaching solar radiation. The transport of dust aerosol on 12 April 2007, 27 April 2007, 1 June 2007, 4 June 2009 and 19 June 2009 cause a significant reduction in the surface-reaching short-wave solar radiation by 43, 40, 39, 50 and 42 Wm^{-2} , respectively. This increased the atmospheric forcing on these days by 33.8, 33, 33.2, 35.3 and 30.1 Wm^{-2} , respectively, which translates into an atmospheric heating rate of 0.95, 0.93, 0.93, 0.99 and 0.84 K day^{-1} , respectively. During these days, the aerosol radiative forcing (average of dust loading days) on the SFC, TOA and ATM became -42.8 , -9.5 and 33.1 Wm^{-2} , respectively. The increase in atmospheric forcing due to dust aerosols transport translates into an atmospheric heating rate of 0.93 K day^{-1} . This study estimated that, during dust aerosol transport

days, the average forcing at the SFC and TOA change by -26 and -6 Wm^{-2} , respectively, when compared with the average value of low aerosol loading days, i.e. 21 April 2007 and 10 April 2009. This implies a significant reduction in the surface-reaching solar radiation by 149%. This large reduction in the surface-reaching solar radiation increases the atmospheric heating rate by a factor of 2.4. During dust event period, Prasad et al. (2007) presented the results from Kanpur located in the IGP to investigate the influence of aerosol transport on surface-reaching short-wave solar radiation. That study found that, during dusty days, the average forcing at the SFC and TOA change by -23 and -11 Wm^{-2} , respectively.

This study of aerosol transport has revealed that Mohal is representative of two different types of aerosols, which presents two characteristic atmospheric situations over the region. This section describes the influence of the long-range transport of anthropogenic aerosols on incoming solar radiation. From Fig. 8c, it is made clear that the transport of anthropogenic aerosol on 25 October 2007, 11 October 2008 and 19 October 2009 caused a significant reduction in the surface-reaching short-wave solar radiation by 33.4 , 35.2 and 56.6 Wm^{-2} , respectively. This increased the atmospheric forcing on these days by 22 , 24.4 and 31 Wm^{-2} , respectively, which translates into an atmospheric heating rate of 0.62 , 0.68 and 0.87 K day^{-1} , respectively. During these days, the aerosol radiative forcing (average of dust or polluted dust and smoke loading days) on the SFC, TOA and ATM became -41.7 , -15.9 and 25.8 Wm^{-2} , respectively. The increase in atmospheric forcing due to polluted dust and smoke aerosols transport translates into an atmospheric heating rate of 0.72 K day^{-1} . This study has estimated a significant reduction in the surface-reaching solar radiation by 117% during dust or polluted dust and smoke aerosol transport days when the result was compared with the average values of low aerosol loading days, i.e. 8 October 2007, 12 October 2008 and 10 October 2009. This large reduction in surface-reaching solar radiation increases the atmospheric heating rate by a factor of 2.

Badarinath et al. (2009) carried out a study during October 2007 over Hyderabad, located in the central region of Peninsular India, to estimate the radiative effect of aerosol. That study investigates a considerable reduction in the surface-reaching solar radiation by 107 Wm^{-2} on high aerosol loading days. This reduction is attributed to the transport of smoke aerosol from agricultural waste burning dominant region. A similar result was also reported by Sharma et al. (2010) during October 2007 from Patiala, with a significant reduction in the surface-reaching solar radiation by 212 Wm^{-2} on high smoke aerosol loading day. Tripathi et al. (2005) estimated the impact of anthropogenic aerosol on solar radiation over Kanpur, with

a decrease in the surface-reaching solar radiation by 62 Wm^{-2} .

5 Conclusion

Ground and satellite observations of aerosol properties are carried out under clear sky days during 2007 to 2009 and are here analysed, together with aerosol trajectories. The summary of the results shows that the daily average value of the aerosol optical depth (AOD) at 500 nm, α and β are 0.24 ± 0.08 , 1.02 ± 0.34 and 0.13 ± 0.05 , respectively. A comparative study of the MWR and MODIS observations reveals that the percentage retrieval for daily AOD at 550 nm over Mohal within the expected accuracy ($\Delta\tau_{p\lambda} = \pm 0.05 \pm 0.15\tau_{p\lambda}$) is around 87%, whereas the expected accuracy with respect to the AERONET-derived AOD over the Indian land is 90%. MODIS- and MWR-derived AOD showed good agreement for daily observations, with 0.05, 0.04 and 0.76 for the RMSD, MABD and correlation coefficient, respectively. The absolute difference in the AOD is observed as 0.01. The present study, therefore, suggests that the MODIS AOD retrievals are able to effectively characterise the AOD distribution over Mohal. However, further efforts to eliminate systematic errors in the existing MODIS algorithm are needed.

Besides local sources, the long-range transport of aerosol also contributes to the existing columnar aerosols. The aerosol transport from different source origins has played a major role in building the aerosol layer over Mohal. The transport of desert dust aerosol has caused a significant reduction in the surface-reaching short-wave solar radiation by 149%. This reduction in the surface-reaching solar radiation increased the atmospheric heating rate by a factor of 2.4. The transport of anthropogenic aerosols (polluted dust and smoke) caused a significant reduction in the surface-reaching short-wave solar radiation by 117%. This reduction in the surface-reaching solar radiation increased the atmospheric heating rate by a factor of 2. This study indicates significant climatic implications due to the transport of aerosols in the northwestern Indian Himalaya.

Acknowledgements The authors thank the Director, G.B. Pant Institute of Himalayan Environment and Development, Kosi-Katarmal, Almora, Uttarakhand, for providing the necessary facilities. The authors are grateful to the Indian Space Research Organization (ISRO), Bangalore, for providing financial assistance to this project through the Space Physics Laboratory, Vikram Sarabhai Space Centre (VSSC), Thiruvananthapuram, Kerala. We acknowledge National Aeronautics and Space Administration (NASA) for providing the Moderate Resolution Imaging Spectroradiometer (MODIS) and Cloud Aerosol Lidar and Infrared Pathfinder Satellite Observations (CALIPSO) aerosol data and the National Oceanic and Atmospheric Administration (NOAA) Air Resources Laboratory for a provision of the HYbrid Single-Particle Lagrangian Integrated Trajectory

(HYSPLIT) transport and dispersion model which we have used in this publication. We thank the reviewers for their constructive comments and suggestions.

References

- Aloysius M, Mohan M, Parameswaran K, George SK, Nair PR (2008) Aerosol transport over the Gangetic basin during ISRO-GBP land campaign-II. *Ann Geophys* 26:431–440
- Ångström A (1961) Techniques of determining the turbidity of the atmosphere. *Tellus* 13:214–223
- Babu SS, Moorthy KK, Satheesh SK (2007) Temporal heterogeneity in aerosol characteristics and the resulting radiative impacts at a tropical coastal station—Part 2: direct short wave radiative forcing. *Ann Geophys* 25:2309–2320
- Badarinath KVS, Kharol SK, Kaskaoutis DG, Kambezidis HD (2007) Case study of a dust storm over Hyderabad area, India: its impact on solar radiation using satellite data and ground measurements. *Sci Tot Environ* 384:316–332
- Badarinath KVS, Kharol SK, Prasad VK, Sharma AR, Reddi EUB, Kambezidis HD, Kaskaoutis DG (2008) Influence of natural and anthropogenic activities on UV Index variations—a study over tropical urban region using ground based observations and satellite data. *J Atmos Chem* 59:219–236
- Badarinath KVS, Kharol SK, Sharma AR (2009) Long-range transport of aerosols from agriculture crop residue burning in Indo-Gangetic Plains—a study using LIDAR, ground measurements and satellite data. *J Atmos Sol Terr Phys* 71:112–120
- Beegum SN, Moorthy KK, Nair VS, Babu SS, Satheesh SK, Vinoy V, Reddy RR, Gopal KR, Badarinath KVS, Niranjan K, Pandey SK, Behera M, Jeyaram A, Bhuyan PK, Gogoi MM, Singh S, Pant P, Dumka UC, Kant Y, Kuniyal JC, Singh D (2008) Characteristics of spectral aerosol optical depths over India during ICARB. *J Earth Syst Sci* 117(S1):303–313
- Bellouin N, Boucher O, Haywood J, Reddy MS (2005) Global estimate of aerosol direct radiative forcing from satellite measurements. *Nature* 438:1138–1141
- Bollasina M, Nigam S (2009) Absorbing aerosols and pre-summer monsoon hydroclimate variability over the Indian subcontinent: the challenge in investigating links. *Atmos Res* 94:338–344
- Charlson RJ, Schwartz SE, Hales JM, Cess RD, Coakley JA, Hansen JE, Hoffman DJ (1992) Climate forcing by anthropogenic aerosols. *Science* 255:423–430
- Chu DA, Kaufman YJ, Remer LA, Holben BN (1998) Remote sensing of smoke from MODIS airborne simulator during the SCAR-B experiment. *J Geophys Res* 103:31979–31987
- Chu DA, Kaufman YJ, Ichoku C, Remer LA, Tanré D, Holben BN (2002) Validation of MODIS aerosol optical depth retrieval over land. *Geophys Res Lett* 29:8007. doi:10.1029/2001GL013205
- Deschamps P-Y, Bréon F-M, Leroy M, Podaire A, Bricaud A, Buriez J-C, Sèze G (1994) The POLDER mission: instrument characteristics and scientific objectives. *IEEE Trans Geosci Remote Sens* 32:598–615
- Dey S, Tripathi SN, Singh RP, Holben BN (2004) Influence of dust storms on the aerosol optical properties over the Indo-Gangetic basin. *J Geophys Res* 109:D20211. doi:10.1029/2004JD004924
- Draxler RR, Rolph GD (2010) HYbrid Single-Particle Lagrangian Integrated Trajectory (HYSPLIT) Model. Access via NOAA ARL READY Website, NOAA Air Resources Laboratory, Silver Spring, MD, USA. <http://ready.arl.noaa.gov/HYSPLIT.php>
- Eck TF, Holben BN, Reid JS, Dubovik O, Smirnov A, O’Neil NT, Slutsker I, Kinne S (1999) Wavelength dependence of the optical depth of biomass burning, urban, and desert dust aerosols. *J Geophys Res* 104:31333–31349
- Fu Q, Liou KN (1992) On the correlated *k*-distribution method for radiative transfer in nonhomogeneous atmospheres. *J Atmos Sci* 49:2139–2156
- Fu Q, Liou KN (1993) Parameterization of the radiative properties of cirrus clouds. *J Atmos Sci* 50:2008–2025
- Ganesh KE, Umesh TK, Narasimhamurthy B (2005) On the relationship between the Ångström’s turbidity parameters. *IASTA Bull* 17:527–528
- Gautam R, Hsu NC, Lau K-M, Kafatos M (2009) Aerosol and rainfall variability over the Indian monsoon region: distributions, trends and coupling. *Ann Geophys* 27:3691–3703
- Gogoi MM, Bhuyan PK, Moorthy KK (2008) Estimation of the effect of long-range transport on seasonal variation of aerosols over northeastern India. *Ann Geophys* 26:1365–1377
- Gogoi MM, Bhuyan PK, Moorthy KK (2009) An investigation of aerosol size distribution properties at Dibrugarh: North-Eastern India. *Terr Atmos Ocean Sci* 20(3):521–533
- Hoppel WA, Fitzgerald JW, Frick GM, Larson RE, Mack EJ (1990) Aerosol size distributions and optical properties found in the marine boundary layer over the Atlantic Ocean. *J Geophys Res* 95:3659–3686
- Huang J, Minnis P, Yi Y, Tang Q, Wang X, Hu Y, Liu Z, Ayers K, Trepte C, Winker D (2007) Summer dust aerosols detected from CALIPSO over the Tibetan Plateau. *Geophys Res Lett* 34:L18805. doi:10.1029/2007GL029938
- Huang J, Minnis P, Chen B, Huang Z, Liu Z, Zhao Q, Yi Y, Ayers JK (2008) Long-range transport and vertical structure of Asian dust from CALIPSO and surface measurements during PACDEX. *J Geophys Res* 113:D23212. doi:10.1029/2008JD010620
- Huang J, Fu Q, Su J, Tang Q, Minnis P, Hu Y, Yi Y, Zhao Q (2009) Taklimakan dust aerosol radiative heating derived from CALIPSO observations using the Fu-Liou radiation model with CERES constraints. *Atmos Chem Phys* 9:4011–4021
- Ichoku C, Remer LA, Kaufman YJ, Levy R, Chu DA, Tanré D, Holben BN (2003) MODIS observation of aerosols and estimation of aerosol radiative forcing over southern Africa during SAFARI 2000. *J Geophys Res* 108:8499. doi:10.1029/2002JD002366
- Intergovernmental Panel on Climate Change (IPCC) (2007) Climate change 2007—the physical science basis. Cambridge University Press, Cambridge
- Iqbal M (1983) An introduction to solar radiation. Academic Press, New York
- Jacovides CP, Kaltsounides NA, Asimakopoulos DN, Kaskaoutis DG (2005) Spectral aerosol optical depth and Ångström parameters in the polluted Athens atmosphere. *Theor Appl Climatol* 81:161–167
- Jayaraman A, Ratnam MV, Patra AK, Rao TN, Sridharan S, Rajeevan M, Gadhave H, Kesarkar AP, Srinivasulu P, Raghunath K (2010) Study of Atmospheric Forcing and Responses (SAFAR) campaign: overview. *Ann Geophys* 28:89–101
- Kaskaoutis DG, Kambezidis HD, Hatzianastassiou N, Kosmopoulos PG, Badarinath KVS (2007) Aerosol climatology: dependence of the Ångström exponent on wavelength over four AERONET sites. *Atmos Chem Phys Discuss* 7:7347–7397
- Kaskaoutis DG, Badarinath KVS, Kharol SK, Sharma AR, Kambezidis HD (2009) Variations in the aerosol optical properties and types over the tropical urban site of Hyderabad, India. *J Geophys Res* 114:D22204. doi:10.1029/2009JD012423
- Kaskaoutis DG, Kosmopoulos PG, Kambezidis HD, Nastos PT (2010) Identification of the aerosol types over Athens, Greece: the influence of air-mass transport. *Adv Meteorol*, article ID 168346. doi:10.1155/2010/168346
- Kaufman YJ, Hobbs PV, Kirchhoff VWJH, Artaxo P, Reme LA, Holben BN, King MD, Ward DE, Prins EM, Longo KM, Mattos LF, Nobre CA, Spinhirne JD, Ji Q, Thompson AM, Gleason JF,

- Christopher SA, Tsay SC (1998) Smoke, Clouds, and Radiation—Brazil (SCAR-B) experiment. *J Geophys Res* 103(D24): 31783–31808
- Kaufman YJ, Gobron N, Pinty B, Widlowski J-L, Verstraete MM (2002) Relationship between surface reflectance in the visible and mid-IR used in MODIS aerosol algorithm—theory. *Geophys Res Lett* 29(23):2116. doi:[10.1029/2001GL014492](https://doi.org/10.1029/2001GL014492)
- Kedia S, Ramachandran S (2008) Latitudinal and longitudinal variation in aerosol characteristics from Sun photometer and MODIS over the Bay of Bengal and Arabian Sea during ICARB. *J Earth Syst Sci* 117:375–387
- Kedia S, Ramachandran S (2009) Variability in aerosol optical and physical characteristics over the Bay of Bengal and the Arabian Sea deduced from Ångström exponents. *J Geophys Res* 114:D14207. doi:[10.1029/2009JD011950](https://doi.org/10.1029/2009JD011950)
- Kedia S, Ramachandran S, Kumar A, Sarin MM (2010) Spatiotemporal gradients in aerosol radiative forcing and heating rate over Bay of Bengal and Arabian Sea derived on the basis of optical, physical, and chemical properties. *J Geophys Res* 115:D07205. doi:[10.1029/2009JD013136](https://doi.org/10.1029/2009JD013136)
- King MD, Kaufman YJ, Tanré D, Nakajima T (1999) Remote sensing of tropospheric aerosols from space: past, present, and future. *Bull Am Meteorol Soc* 80:2229–2259
- Kuniyal JC, Rao PSP, Momin GA, Safai PD, Tiwari S, Ali K (2007) Trace gases behaviour in sensitive areas of the northwestern Himalaya—a case study of Kullu-Manali tourist complex, India. *Indian J Radio Space Phys* 36:197–203
- Kuniyal JC, Thakur A, Thakur HK, Sharma S, Pant P, Rawat PS, Moorthy KK (2009) Aerosol optical depths at Mohal-Kullu in the northwestern Indian Himalayan high altitude station during ICARB. *J Earth Syst Sci* 118(1):41–48
- Lau KM, Kim MK, Kim KM (2006) Asian summer monsoon anomalies induced by aerosol direct forcing: the role of the Tibetan Plateau. *Clim Dyn* 26:855–864
- Levy RC, Remer LA, Dubovik O (2007) Global aerosol optical properties and application to Moderate Resolution Imaging Spectroradiometer aerosol retrieval over land. *J Geophys Res* 112:D13210. doi:[10.1029/2006JD007815](https://doi.org/10.1029/2006JD007815)
- Liou KN (2002) An introduction to atmospheric radiation. Elsevier, New York
- Liu Z, Liu D, Huang J, Vaughan M, Uno I, Sugimoto N, Kittaka C, Trepte C, Wang Z, Hostetler C, Winker D (2008) Airborne dust distributions over the Tibetan Plateau and surrounding areas derived from the first year of CALIPSO lidar observations. *Atmos Chem Phys* 8:5045–5060
- Menon S, Hansen J, Nazarenko L, Luo Y (2002) Climate effects of black carbon aerosols in China and India. *Science* 297:2250–2253
- Middleton NJ (1986) A geography of dust storms in southwest Asia. *Int J Climatol* 6:183–196
- Misra A, Jayaraman A, Ganguly D (2008) Validation of MODIS derived aerosol optical depth over Western India. *J Geophys Res* 113:D04203. doi:[10.1029/2007JD009075](https://doi.org/10.1029/2007JD009075)
- Misra A, Jayaraman A, Ganguly DA (2010) A comparative study of MODIS derived aerosol optical depth from two consecutive versions. *IASTA Bull* 19:212
- Moorthy KK, Nair PR, Murthy BVK (1991) Size distribution of coastal aerosols: effects of local sources and sinks. *J Appl Meteorol* 30:844–852
- Moorthy KK, Nair PR, Murthy BVK, Satheesh SK (1996) Time evolution of the optical effects and aerosol characteristics of Mt. Pinatubo origin from ground-based observations. *J Atmos Terr Phys* 58(10):1101–1116
- Moorthy KK, Satheesh SK, Murthy BVK (1998) Characteristics of spectral optical depths and size distributions of aerosols over tropical oceanic regions. *J Atmos Sol Terr Phys* 60(10):981–992
- Moorthy KK, Niranjana K, Narasimhamurthy B, Agashe VV, Murthy BVK (1999) Aerosol climatology over India. ISRO-GBP MWR network and data base. Scientific report, SR-03–99. Indian Space Research Organisation (ISRO), Bangalore
- Morales C (1986) The airborne transport of Saharan dust: a review. *Clim Change* 9:219–241
- Myhre G, Govaerts Y, Haywood JM, Bernsten TK, Lattanzio A (2005) Radiative effect of surface albedo change from biomass burning. *Geophys Res Lett* 32:L20812. doi:[10.1029/2005GL022897](https://doi.org/10.1029/2005GL022897)
- Narasimhamurthy B, Raju NV, Tukarama M, Prasad BSN, Moorthy KK (1998) Studies of the temporal and spectral features of atmospheric aerosols over Mysore (12.3.-N), Global Change Studies, ISRO-GBP: GSC-02-98:77–92
- Parameswaran K, Nair PR, Rajan R, Ramana MV (1999) Aerosol loading in coastal and marine environments in the Indian Ocean region during winter season. *Curr Sci* 76(7):947–955
- Pathak B, Bhuyan PK, Gogoi MM, Kalita G, Bhuyan K (2010) Validation of satellite derived AOD by ground based observation over Dibrugarh. *IASTA Bull* 19:219–222
- Powell KA, Hostetler CA, Vaughan MA, Kuehn RE, Hunt WH, Lee K-P, Trepte CR, Rogers RR, Young SA, Winker DM (2009) CALIPSO Lidar calibration algorithms. Part I: nighttime 532-nm parallel channel and 532-nm perpendicular channel. *J Atmos Oceanic Technol* 26(10):2015–2033
- Prasad AK, Singh S, Chauhan SS, Srivastava MK, Singh RP, Singh R (2007) Aerosol radiative forcing over the Indo-Gangetic plains during major dust storms. *Atmos Environ* 41:6289–6301
- Prasad AK, Yang K-HS, El-Askary HM, Kafatos M (2009) Melting of major Glaciers in the western Himalayas: evidence of climatic changes from long term MSU derived tropospheric temperature trend (1979–2008). *Ann Geophys* 27:4505–4519
- Prospero JM, Ginoux P, Torres O, Nicholson SE, Gill TE (2002) Environmental characterization of global sources of atmospheric soil dust identified with the Nimbus 7 Total Ozone Mapping Spectrometer (TOMS) absorbing aerosol product. *Rev Geophys* 40:1002. doi:[10.1029/2000RG000095](https://doi.org/10.1029/2000RG000095)
- Raju NV, Prasad BSN, Narasimhamurthy B (2003) Atmospheric aerosols and air pollution. *Indian J Radio Space Phys* 32:306–311
- Ramachandran S, Rengarajan R, Jayaraman A, Sarin MM, Das SK (2006) Aerosol radiative forcing during clear, hazy, and foggy conditions over a continental polluted location in north India. *J Geophys Res* 111:D20214. doi:[10.1029/2006JD007142](https://doi.org/10.1029/2006JD007142)
- Ramanathan V, Crutzen PJ, Holben B, Priestley K, Lelieveld J, Mitra AP, Althausen D, Anderson J, Andreae MO, Cantrell W (2001) Indian Ocean Experiment: an integrated analysis of the climate forcing and effects of the great Indo-Asian haze. *J Geophys Res* 106:28371–28398
- Ramanathan V, Chung C, Kim D, Bettge T, Buja L, Kiehl JT, Washington WM, Fu Q, Sikka DR, Wild M (2005) Atmospheric brown clouds: impacts on South Asian climate and hydrological cycle. *Proc Natl Acad Sci USA* 102:5326–5333
- Ranjan RR, Joshi HP, Iyer KN (2007) Spectral variation of total column aerosol optical depth over Rajkot: a tropical semi-arid Indian station. *Aerosol Air Qual Res* 7(1):33–45
- Remer LA, Kaufman YJ, Tanré D, Mattoo S, Chu DA, Martins J, Li R-R, Ichoku C, Levy RC, Kleidman RG, Eck TF, Vermote E, Holben BN (2005) The MODIS aerosol algorithm, products, and validation. *J Atmos Sci* 62(4):947–973
- Rienecker MM, Suarez MJ, Todling R, Bacmeister J, Takacs L, Liu H-C, Gu W, Sienkiewicz M, Koster RK, Gelaro R, Stajner I, Nielsen JE (2008) The GEOS-5 data assimilation system—documentation of versions 5.0.1, 5.1.0, and 5.2.0, NASA Technical Report Series on Global Modeling and Assimilation, NASA/T-2008–104606, Vol. 27. NASA Goddard Space Flight Center: Greenbelt, MA, USA.

- Russell PB, Livingston JM, Dutton EG, Pueschel V, Reagon JA, Defoor TE, Box MA, Allen D, Pilewskie P, Herman BM, Kinnie SA, Hofmann DJ (1993) Pinatubo and pre-pinatubo optical-depth spectra: Mauna Loa measurements, comparisons, inferred particle size distributions, radiative effects, and relationship to Lidar data. *J Geophys Res* 98:22969–22985
- Sagar R, Kumar B, Dumca UC, Moorthy KK, Pant P (2004) Characteristics of aerosol spectral optical depths over Manora Peak: a high-altitude station in the central Himalaya. *J Geophys Res* 109:D06207. doi:10.1029/2003JD003954
- Saha A, Moorthy KK, Niranjan K (2005) Interannual variations of aerosol optical depth over coastal India: relation to synoptic meteorology. *J Appl Meteor* 44:1066–1077
- Satheesh SK, Ramanathan V (2000) Large differences in the tropical aerosol forcing at the top of the atmosphere and Earth's surface. *Nature* 405:60–63
- Satheesh SK, Moorthy KK, Das I (2001) Aerosol spectral optical depths over the Bay of Bengal, Arabian Sea and Indian Ocean. *Curr Sci* 81(12):1617–1625
- Satheesh SK, Ramanathan V, Holben BN, Moorthy KK, Loeb NG, Maring H, Prospero JM, Savoie D (2002) Chemical, microphysical, and radiative effects of Indian Ocean aerosols. *J Geophys Res* 107(D23):4725. doi:10.1029/2002JD002463
- Schuster GL, Dubovik O, Holben BN (2006) Ångström exponent and bimodal aerosol size distributions. *J Geophys Res* 111:D07207. doi:10.1029/2005JD006328
- Sharma NL, Kuniyal JC, Singh M, Negi AK, Singh K, Sharma P (2009) Number concentration characteristics of ultrafine aerosols (atmospheric nanoparticles/aitken nuclei) during 2008 over western Himalayan region, Kullu-Manali, India. *Indian J Radio Space Phys* 38:326–337
- Sharma AR, Kharol SK, Badarinath KVS, Singh D (2010) Impact of agriculture crop residue burning on atmospheric aerosol loading—a study over Punjab State, India. *Ann Geophys* 28:367–379
- Shaw GE, Reagan JA, Herman BM (1973) Investigations of atmospheric extinction using direct solar radiation measurements made with a multiple wavelength radiometer. *J Appl Meteorol* 12:374–380
- Singh RP, Dey S, Tripathi SN, Tare V, Holben B (2004) Variability of aerosol parameters over Kanpur, northern India. *J Geophys Res* 109:D23206. doi:10.1029/2004JD004966
- Tripathi SN, Dey S, Chandel A, Srivastava S, Singh RP, Holben BN (2005) Comparison of MODIS and AERONET derived aerosol optical depth over the Ganga Basin, India. *Ann Geophys* 23:1093–1101
- Vinoj V, Satheesh SK, Moorthy KK (2008) Aerosol characteristics at a remote island: Minicoy in southern Arabian Sea. *J Earth Syst Sci* 117:389–397
- Yu H, Dickinson RE, Chin M, Kaufman YJ, Zhou L, Tian Y, Dubovik O, Holben BN (2004) Direct radiative effect of aerosols as determined from a combination of MODIS retrievals and GOCART simulations. *J Geophys Res* 109:D03206. doi:10.1029/2003JD003914
- Zhao TX-P, Stowe LL, Smirnov A, Crosby D, Sapper J, McClain CR (2002) Development of a global validation package for satellite oceanic aerosol optical thickness retrieval based on AERONET observations and its application to NOAA/NESDIS operational aerosol retrievals. *J Atmos Sci* 59:294–312